Title

Reduction of Cox6a2 in PV+ interneurons decreases neuronal firing rate and frequency of theta and gamma oscillations and increases place field size in the CA1 region of the hippocampus

Author

Patel, Rina

Publication Date

2020

Peer reviewed|Thesis/dissertation

UNIVERSITY OF CALIFORNIA SAN DIEGO

Reduction of Cox6a2 in PV+ interneurons decreases neuronal firing rate and frequency of theta and gamma oscillations and increases place field size in the CA1 region of the hippocampus

A Thesis submitted in partial satisfaction of the requirements for the degree

Master of Science

in

Biology

by

Rina Patel

Committee In Charge:

Professor Stefan Leutgeb, Chair
Professor Gulcin Pekkurnaz, Co-Chair
Professor Byungkook Lim

2020

SIGNATURE PAGE

The Thesis of Rina Patel is approved, and it is acceptable in quality and form for publication on microfilm and electronically:

Chair

University of California San Diego

2020

DEDICATION

I would like to dedicate this thesis to my mother, Bharti Patel. Mom, your work ethic and unwavering perseverance through the struggles you have faced gives me the inspiration and strength I have today. Thank you for everything. To you, I dedicate not only this thesis, but all and any accomplishments I have and will achieve.

TABLE OF CONTENTS

LIST OF FIGURES

ACKNOWLEDGEMENTS

I would like to acknowledge the principal investigator for the lab where I completed my thesis, Stefan Leutgeb. Thank you for acting as the chair of my committee and giving me patience, advice, and encouragement as I worked on my project. Your guidance while I began my path to become a researcher was filled with incomparable knowledge and experience that I will forever cherish. The constant guidance you gave me while I was writing this thesis has taught me how to be a better communicator, writer, and researcher. Thank you for believing in me and for trusting me with this project.

I would also like to acknowledge Professor Gulcin Pekkurnaz for serving as the co-chair on my committee. Your enthusiasm and passion for this project was incredibly influential in pushing me and keeping me excited about this project. I also thank Professor Byungkook Lim for serving on my committee as well. Without your support, this project would not come as far as it did.

I must also acknowledge everyone who I had the pleasure of interacting throughout my time in the Leutgeb lab. First, I would like to thank you Jill Leutgeb. Your advice on my data during our lab meetings helped shape how I show my data for this thesis. Next, I thank my first friend in the lab, Max Ledakis. I would also like to thank Kshitij Gaur, for being a kind friend to me in the lab who I could always talk to. Being a witness to you complete your masters inspired me to do the same, and I would not be here without your help, support, and encouragement. I am also very grateful for Maylin Fu for welcoming me into the lab and teaching me many of the important techniques I utilized throughout my experiments. Without your wealth of experience and knowledge, I would not have been able to make the progress I did. I am most grateful for

Naomie Devico-Marciano. Thank you for pushing me when I started to lag, motivating me when I was exhausted, and supporting me when I was at my low points. Without you embarking on a similar journey with me, the master's program would not have been as bearable or joyful as it turned out to be. I would also like to thank Li Yuan, who was generous enough to write code for us that allowed us to analyze our place field data.

I would also like to acknowledge COVID-19, for being the largest obstacle I faced during my master's program journey. I was unsure if I could overcome you, but in the end, I prevailed, and I managed to complete my master's thesis despite you.

I also have to thank my family and friends outside of the lab who influenced my journey. Thank you to my Flagstaff crew, Pooja Sangha, Mia Armstrong, Jonathan Kim, and Chance Marostica, for weekly zoom meetings that boosted my moral during the last phases of my master's. I would also like to sincerely thank Karthik Arunachalam for all the kindness and encouragement you provided me since I began my master's program. Thank you for also reviewing my figures to make sure they were up to standard and distracting me when I was overworking.

Finally, I would like to thank my mentor and confidant during this process, Dr. Silvia Viana da Silva. I am so honored to have you in my life. You have truly been a hero to me. No matter how busy you were, you always stopped to answer my millions of questions (which I either later found in papers or asked again and again). You stood with me in support and encouragement when I was at my lowest points. Without you, this thesis would have been nonexistent, much like my pursuit of a master's degree and my entrance into the field of neuroscience. When it began to feel as though I was taking your inspiring presence for granted, we faced COVID-19 during our last stretch at UCSD which shut down the world. As a witness to you battling with a one-year old child due to no healthcare, 15 six-month old mice who had too many amazing cells, an expiring visa, a

major international move, and sleep deprivation, I was inspired once more. How you made those struggles (which would have crippled me) look manageable, while looking flawless in the process, is a mystery to me. I would also like to thank Matthias Haberl, who is the reason we were able to have code to analyze most our data. You also had to face the struggle of raising a one-year old child in the midst of a pandemic, especially while Silvia had to tend to her many mice, all while helping me wrap up my data analysis for this thesis. I do not know how I can express how deeply grateful I am for you both. Perhaps how I have described our hard work in this thesis can suffice for now.

This thesis is being used to prepare a submission of publication of material by Silvia Viana da Silva; Luczak, Vince; Haberl, Matthias; Shin, Sora; Lim, Byungkook; Pekkurnaz, Gulcin; Leutgeb, Stefan. The thesis author will be a co-author of the publication.

ABSTRACT OF THE THESIS

Reduction of Cox6a2 in PV+ interneurons decreases neuronal firing rate and frequency of theta and gamma oscillations and increases place field size in the CA1 region of the hippocampus

by

Rina Patel

Master of Science in Biology

University of California San Diego, 2020

Professor Stefan Leutgeb, Chair

Assistant Professor Gulcin Pekkurnaz, Co-Chair

Within the hippocampus, a subclass of interneurons known as parvalbumin positive (PV+) interneurons, play an important role in generating neural oscillations and in influencing the firing rate of pyramidal cells. To maintain such an extensive control, PV+ interneurons have a high energy demand, but how PV+ interneurons are able to generate enough energy is not well understood. Previous studies have shown that dysregulations in mitochondrial subunits, Cox6a1 and Cox6a2, have impaired the activity of complex IV within mitochondria. In this study, we investigate Cox6a1 and Cox6a2 to understand their contribution to mitochondrial function in

PV+ interneurons and whether they are necessary for PV+ interneurons to maintain function. Through an AAV-miR construct, we were able to successfully reduce levels of Cox6a1 and Cox6a2 within PV+ interneurons selectively in the CA1 region of the mouse hippocampus. Electrophysiological recordings from that region revealed that reducing Cox6a1 did not have an effect on the firing rate of interneurons and pyramidal cells or neural oscillations generated in CA1 but did increase the number and size of place fields. Reducing Cox6a2 decreased the firing rate of pyramidal cells, decreased the frequency of theta and gamma oscillations, and also increased the number and size of place fields. Because reducing levels of Cox6a2 in PV+ interneurons disrupted neuronal oscillations and neuronal firing patterns in the hippocampus, this suggests that hippocampus-dependent memory function relies on a specialized regulation of mitochondrial activity in PV+ interneurons.

INTRODUCTION

The brain relies on a vast interconnected network of cells, composed of neurons and glia, to allow for complex cognitive processes. Understanding these networks and how they function has been the goal of scientists since Golgi and Ramón y Cajal mapped the first neuronal networks in the 19th century (Cajal, 1894; Golgi, 1906). Since then, we have come a long way in our understanding and appreciation of the way neurons are connected and communicate with one another. At the highest level, communication between neurons gives rise to cognitive function (Hartley et al., 2014), and the underlying mechanisms are only beginning to be understood. This is because it requires studying the many networks that make up the brain, as well as the mechanisms and individual differences within the neurons that make up those networks (Power et al., 2010; Sporns et al., 2005). Recent advances in fluorescence staining, recording techniques, and biological manipulations have increased the ability for the brain networks to be studied. One of the brain regions has been extensively manipulated and studied is the rodent hippocampus.

The hippocampus is widely studied for its role in memory consolidation, encoding episodic memory, and spatial memory and navigation (Broadbent et al., 2004). It is composed of three main subregions, known as CA1, CA3, and the dentate gyrus (DG) (Deshmukh & Knierim, 2012). Within these subregions are many different types of neurons that create a densely interconnected neuronal networks (Van Strien et al., 2009). The neurons located in the DG project out to the CA3 region. The neurons within the CA3 region project back onto CA3 neurons, DG neurons, and out to neurons in CA1 (Witter et al., 2006). The neurons in the CA1 region project back onto CA1 neurons and out to other brain regions, such as the subiculum. The neurons that make up these three subregions are known as the "hippocampus proper." The hippocampus proper communicates with neighboring brain structures which are also essential for its role in memory, such as the

entorhinal cortex and subiculum. The DG neurons receive input from the superficial layers of the entorhinal cortex. CA1 also receives input directly from the entorhinal cortex and sends out projections to the subiculum and the deep layers of the entorhinal cortex. Understanding the roles of the different types of neurons that make up the hippocampus is essential to understanding how this network allows for memory processes to occur.

As is the case for all brain regions, the hippocampus proper is composed of two main groups of neurons: excitatory neurons and inhibitory neurons (Prestigio et al., 2019). The excitatory neurons are classified as those that release the neurotransmitter glutamate, which causes the membrane potential of postsynaptic neurons to become more positive and thus leads to increased neuronal activity. The inhibitory neurons are classified as those that release the neurotransmitter GABA, which drives the membrane potential of postsynaptic neurons to -70mV and therefore leads to decreased neuronal activity. The main glutamatergic excitatory neurons are referred to as 'pyramidal cells' (Zeisel et al., 2015), due to the pyramid shape of their cell bodies. The axons and dendrites of pyramidal cells can spread out through different layers of the hippocampus, allowing them to send and receive information across different layers (Hartley et al., 2014). Most GABAergic inhibitory neurons are local interneurons with connections within a hippocampal subregion (Bezaire & Soltesz, 2013). The axons and dendrites of GABAergic interneurons, are localized within individual layers, allowing them to receive and send information "locally". There are over 21 different subtypes of inhibitory interneurons in the CA1 region alone, of which the majority are PV+ interneurons, characterized by the presence of a calcium-binding protein, parvalbumin (PV) (Bezaire & Soltesz, 2013; Hu et al., 2014; Klausberger & Somogyi, 2008; Moser, 2003). These interneurons display high frequency fast spiking characteristics which allow them to produce high amplitude action potentials in a short time period (Ferguson, 2018).

The interaction of the excitatory pyramidal cells and the inhibitory PV+ interneurons work to regulate the activity of neurons in the hippocampus, which plays an important role in allowing information to be received and sent out of the hippocampus (Buzsáki et al., 2007).

The periods of inhibition and excitation generated by interaction of pyramidal cells and PV+ interneurons occur at specific times relative to each other and generate oscillations in the hippocampus (Atallah & Scanziani, 2009; Cobb et al., 1995; McBain, 2001; Sohal et al., 2009). There are three main types of oscillations that take place: theta (~4-12 Hz) (Colgin, 2016), gamma (~25-100 Hz) (Buzsaki, 1983; Buzsaki, 1986), and sharp wave-ripples (~110-250 Hz) (Buzsaki, 1983; Bragin, 1995). The interaction between excitatory pyramidal cells and inhibitory PV+ interneurons plays an important role in generating gamma and sharp-wave ripples within the CA1 region (Fries et al., 2007; Gan, 2017; Whittington et al., 2000). Gamma oscillations are thought to play an important role in storing and retrieving memories in the hippocampus (Bartos et al., 2007). Sharp wave-ripples are coupled events that occur as a consequence of major excitation by the pyramidal cells CA3 projecting to CA1, which generates a "sharp wave (~0.01-3 Hz)," and bursts of inhibition by the GABAergic interneurons in CA1, which creates the "ripple" (140-200 Hz) (Colgin, 2016; Deshmukh & Knierim, 2012; Schlingloff et al., 2014). Sharp wave-ripples (SWRs) are widely thought to support memory encoding, as the selective disruption or elimination of them are known to impair memory acquisition (Girardeau, 2009).

Gamma oscillations have been previously shown to depend on properly functioning mitochondria to sustain the oscillations (Kann et al., 2011; Whittaker et al., 2011). It has also been shown that periods of inhibition, caused the activation of by PV+ interneurons which, play a key role in generating gamma oscillations (Cardin et al., 2009; Ferguson & Gao, 2018; Gulyás et al., 2010; Sohal et al., 2009). While pyramidal cells can expend high amounts of energy over long

periods of time, PV+ interneurons have a high amplitude, fast-spiking phenotype that requires large bouts of energy to be used over shorter periods of time (Buzsáki et al., 2007). For this reason, we hypothesized that the energetics of PV+ interneurons might be tightly linked to the generation of fast oscillations, such as gamma oscillations and SWRs. While not much work has been done to show the importance of mitochondria in producing SWRs, previous studies have reported an impairment of SWRs when PV+ interneurons were inactivated (Gan et al., 2017; Schlingloff et al., 2014). If PV+ interneurons directly impact SWRs, the mechanisms that allow the mitochondria of PV+ interneurons to support this high energy demand needs to be understood.

To understand the mechanisms that alter mitochondrial function, it is important to understand that mitochondria rely on the various protein subunits that make up their function to produce energy. These subunits come together and form complexes that play a direct role in generating ATP, via oxidative phosphorylation. Mitochondrial function has been reported to be impaired in the process of aging and neurodegenerative diseases (Albers & Flint Beal, 2000). It has also been reported that oxidative stress impairs the functions of PV+ interneurons (Steullet et al., 2017). Looking more in depth at the subunits within the mitochondria, it has been shown that complex IV, also known as cytochrome c oxidase, is an essential component in creating the gradient of protons that drive the synthesis of ATP within neurons (Chicherin et al., 2019; Denis, 1986; Li et al., 2006; Wong-Riley, 1989). Interestingly, the mitochondrial Complex IV in PV+ interneurons is unique because it has a high concentration of a specific mitochondrial protein subunit not found in other cells: Cox6a2 (Tasic et al., 2016).

Cox6a2 is a subunit of the cytochrome oxidase complex, also known as Complex IV, of the electron transport chain (Anthony et al., 1993; Kadenbach et al., 1995; Quintens et al., 2013). This complex plays a vital role in producing ATP at the end of cellular respiration. A similar

subunit, Cox6a1, is also present in PV+ interneurons, but unlike Cox6a2, is found more commonly in other neurons throughout the mouse brain. Previous work has shown that genetically disrupting the transcription of Cox6a1 in muscle cells reduces levels of ATP within those cells (Tamiya, 2014). No work has been done on the effect of knocking out either Cox6a1 or Cox6a2 in hippocampal neurons. In this thesis, we set out to determine whether these mitochondrial subunits play an important role in allowing PV+ interneurons to meet the high energy demand that it requires to function.

In this project, we will aim to answer three main experimental questions. First, we aim to determine whether the spiking patterns of hippocampal interneurons and pyramidal cells are altered when levels of Cox6a1 are reduced in the PV+ interneurons. Second, we will ask whether hippocampal oscillations are altered in these knockout mice. Lastly, we will determine whether the aforementioned parameters are changed when levels of Cox6a2 in PV+ interneurons are reduced instead.

By using electrophysiological recording methods, we will be collecting firing rate and neural oscillation data from PV-Cre mice. A viral vector that is selectively activated in Cre-expressing PV+ interneurons will be injected into the CA1 region and is designed to decrease the transcription of Cox6a1 in the affected PV+ interneurons. A similar construct will be used in a viral vector that targets the transcription levels of Cox6a2.

By knocking down Cox6a1 or Cox6a2 in PV+ interneurons in CA1, we strive to identify how this alters firing patterns and oscillations in that region. It is possible that decreasing levels of Cox6a1 affect the ability of PV+ interneurons to produce the high energy that ripples require. If that is not the case, it can be concluded that the other subunit that has not been knocked down, is able to compensate for the loss and generate the required energy despite the reduced Cox6a1 levels.

It is also possible that knocking down one of the subunits will make it so the other is unable to function to meet the energy demands alone, indicating that both need to be present for PV+ interneurons to function properly. By knocking down these proteins, we expect to see a reduction in the firing rate of neurons in the hippocampus. We also expect that the neural oscillations, such as frequency of theta and gamma oscillations and the abundance of sharp wave-ripples, will decrease as well. This would imply that the mitochondrial subunits Cox6a1 and Cox6a2 are necessary for PV+ interneurons to generate enough energy to function properly.

CHAPTER I: METHODS

Subjects

All procedures were approved by the University of California, San Diego Institutional Animal Care and Use Committee. PV-Cre mice were obtained from The Jackson Laboratory [B6; 129P2-Pvalb$^{tm1(cre)Arbr}$/J Stock No: 008069] and bred with wild-type mice to produce 9 male and 9 female mice that were heterozygous for PV-Cre for the experiments. The mice were weaned after 21 days and housed in groups of 3-5 mice per cage in a 12-hr light/dark cycle (7AM – 7PM light, 7PM – 7AM dark). Food and water was available for the mice *ad libitum.* The mice were randomly assigned to each experimental group: control, Cox6a1 knock down (KD), or Cox6a2 KD. Each experimental group was comprised of six animal subjects, of which three were male and three were female. The mice were aged to 2-3 months before they underwent the initial viral vector surgery. Surgical procedures were performed to bilaterally inject a viral vector into the hippocampal CA1 area of each animal, and also to implant a Microdrive containing electrodes that target the hippocampal CA1 area of the right hemisphere.

Viral Vector Injection Surgery

The animals were anesthetized with 5% isoflurane at 0.4L O_2/min in a Plexiglas chamber. Once immobilized, they were mounted onto a stereotaxic frame with a digital axis display. A heating pad was placed under the animals to keep them warm throughout the surgical procedure. To maintain anesthesia, a nose cone was placed around the noses of the mice which delivered ~2% isoflurane at 0.4L O_2/min. A lubricating ophthalmic gel was applied on the eyes of the mice to prevent their eyes from drying out during the surgical procedure. A pair of small blunt scissors were used to shave the fur right above the skull of the mice until the skin underneath was exposed. To disinfect the newly exposed area, iodine and ethanol were applied back-to-back three times

with a cotton tip applicator. Before proceeding any further, a toe-pinch test was performed to ensure the mouse was anesthetized. Once anesthesia was confirmed and the disinfected region was dry, two reference points were made with a black pen, one right after the intersecting point between the eyes and another right after the intersecting point of the ears. Using the reference points as a "start and finish" guide single straight midline incision was made with a sterile No. 10 blade. Sterilized forceps were used to keep the skin flaps apart and expose the underlying skull. A cotton tip applicator was used to absorb any excess blood that may have been on top of the skull. At this point, a light skull-tap test was performed to ensure the head was tightly fitted on the stereotaxic frame and would not move during the rest of the surgery. A drill was attached to the stereotaxic frame and used to locate bregma. Once bregma was located, the digital axis was set to zero. From here, the drill was moved to lambda and the head of the mouse was moved to ensure that both bregma and lambda were less than 0.1 mm different on the z-axis. This ensured the head of the mouse was leveled with respect to the anterior-posterior (y) and dorsal-lateral (x) axes. If the axes were not level, adjustments were made to the positioning of the head and bregma and lambda were re-located until the axes were level. Once the axes were aligned, the drill was moved just above the surface of the skull at the position of -1.85 on the y-axis and +1.50 on the x-axis, with respect to bregma (0,0,0). The drill bit was turned on and slowly lowered until a single hole was drilled through the skull and dura at this location. The drill was then moved to position -1.50 on the x-axis to create another hole at this location while the y-axis remained unchanged. The drill was then switched for a 1 µL glass pipette filled with a viral vector.

The viral vectors used for this experiment were obtained from Dr. Byungkook Lim's lab. The adeno-associated virus (AAV) used for the control group was AAV_{DJ}-EF1α-DIO-EmGFP; the AAV used for the Cox6a1 D group was AAV_{DJ}-EF1α-DIO-EmGFP-miRNA165-Cox6a1; the

AAV used for the Cox6a2 D group was AAV_{DJ}-EF1α-DIO-EmGFP-miRNA254-Cox6a2 (Figure 1). The pipette was moved to the location of one of the drilled holes until the tip of the glass pipette was directly above the brain tissue. If the dura matter was intact after the drilling a small puncture was performed with a needle. The z-axis was zeroed on the digital scale. The glass pipette was then quickly lowered to location -1.35 on the z-axis and ~0.500 µl of the virus was released at minimum pressure. The pipette was left in place for 5 minutes and was then slowly moved out of the brain. The same procedure was completed at the other drilled hole location. An injection with ~0.1 mg/kg of carprofen was given for analgesia. The skin flaps were then stitched together, and the mouse was removed from the stereotaxic frame and placed back in its home cage, which was heated on top of a heating pad to help with the recovery. The mice were left to recover for at least 5 days before the Microdrive implantation surgery. The construct was allowed 3 weeks to express in the CA1 region of the hippocampus before performing the Microdrive recordings.

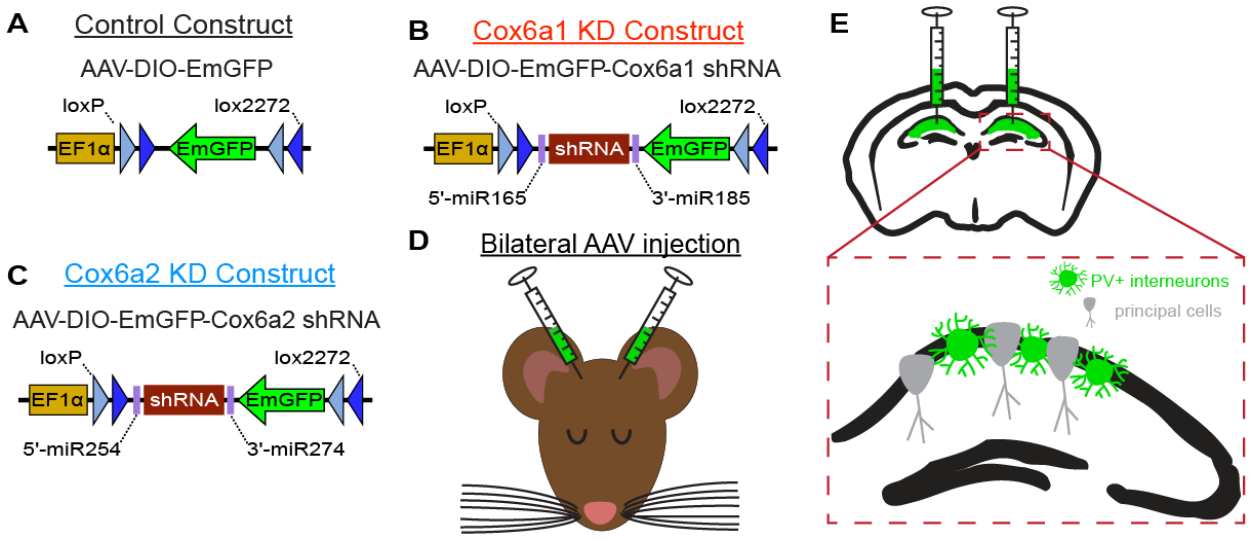

Figure 1. Schematic of the viral vectors bilaterally injected into the hippocampal CA1 region of PV-Cre mice. (A) AAVDJ-EF1α-DIO-EmGFP was injected into the control group. (B) AAVDJ-EF1α-DIO-EmGFP-miRNA165-Cox6a1 was injected into the Cox6a1 KD group. (C) AAVDJ-EF1α-DIO-EmGFP-miRNA254-Cox6a2 was injected into the Cox6a2 KD group. (D) The AAV-EmGFP constructs were bilaterally injected into the CA1 region of the hippocampus in PV-Cre mice. (E) In PV-Cre mice, the Cre-dependent viral vectors resulted in selective expression of the constructs in PV+ interneurons (green) over principal cells (grey).

Microdrive Implantation Surgery

The initial surgical procedures conducted for the Microdrive implantation surgery were identical to the procedures described above for the viral vector injection surgery, up to aligning the head position on the stereotaxic frame. Once the head was properly aligned on the anterior-posterior and dorsal-lateral axes and the digital axis was zeroed at bregma, 4 holes were drilled on the skull around the injection site. A screw was placed halfway in each hole, to support and stabilize the Microdrive (Figure 2). A separate, larger hole was made in the left hemisphere where a ground screw was inserted to contact with the superficial cortical areas. Vetbond was added around the screws to create a strong bond between the screws and the skull, acting as a seal. Once the Vetbond was dry, the Microdrive was attached to the stereotaxic frame and moved until the tip

of the Microdrive was at center of the injection site, right above the brain tissue. The digital z-axis was then zeroed, and the Microdrive was lowered 0.3 mm down along the z-axis. Silicon was added around the base of the Microdrive to seal the tetrodes and the brain tissue. 10 minutes was allotted to cure the silicon, after which dental cement was added to cover the silicon and further secure the Microdrive in place. Once the silicone dried, the mice were removed from the stereotaxic frames, and injected with ~0.1 mg/kg of buprenorphine hydrochloride as a painkiller. The mice were then placed back into their home cages, which were heated with a heating pad to help with recovery.

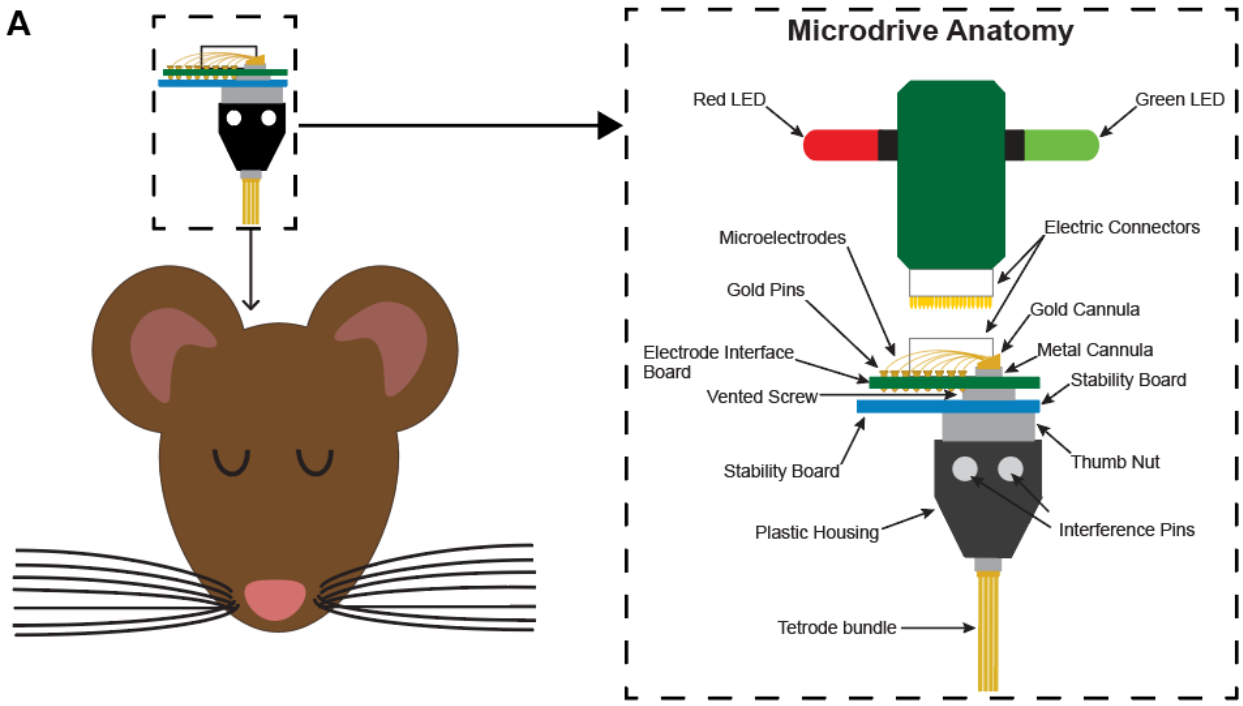

Figure 2. Schematic of the Microdrive Implant. (A) A Microdrive containing 4 tetrodes was surgically implanted in the right hemisphere of the mouse brains, and tetrodes were lowered to the CA1 region of the hippocampus. The Microdrive was connected to an electrophysiological recording system that recorded the single-unit activity and local field potential (LFP) of the CA1 region. The system also tracked the animal's location and head direction via red and green LEDs (the red light was positioned over the mouse's right side of the face and the green light was positioned over the left side of the face).

Electrophysiological Recording Procedure in Freely Behaving Mice

Pre-behavioral training: After the Microdrive implant surgery, while the animals were recovering (5 days), the tetrodes were slowly turned down to decrease the chances of tissue stiffening around the recording sites and causing lesions in the hippocampus with further turning. Every day, the microdrive headset was plugged into a 16-channel Neuralynx data acquisition system via a recording cable, and the local field potential (LFP) and single-unit activity of each animal was observed as the tetrodes were lowered. The Neuralynx system was also connected to a speaker system that allowed for auditory monitoring of the single-unit activity. The tetrodes were lowered slowly over the course of ~2-3 weeks after the Microdrive surgery, adding time for viral expression and for the knock down of RNA to sufficiently alter protein levels.

Behavioral training: As the tetrodes moved closer to the hippocampus, which was manifested as an increase in the amplitude of theta oscillations and by the sounds of bursting cells, the mice underwent three days of behavioral training on an open field. During training, the Microdrive was connected to a preamplifier and cable that forwarded the signal to the Neuralynx data acquisition system, and mice were freely exploring a 60x60 cm^2 box ('open field'). This training familiarized them to the open field environment in which they were placed for the recording sessions, and also helped them become accustomed to moving around with the weight of the recoding cable that was used to connect the Microdrive to the Neuralynx system. The tetrodes for each mouse were still being turned down slowly during this time. Once sharp wave-ripples (SWRs) were observed in conjunction with the presence of unit clusters in the signal that was acquired with the Neuralynx system, daily recording sessions began.

Recordings: Each daily recording session in freely behaving mice began with a 10-minute 'rest' phase, which was followed by running 10 laps on a 100 cm long and 5 cm wide linear track,

then exploring a 60 cm by 60 cm box ('open field') for ~8 minutes and ended with another 10-minute 'rest' phase (Figure 3). During the 'rest' phase, the mice were kept within their home cages which was then placed within a small Plexiglas box to prevent them from climbing out of their cage. Because the animals are often not 'resting' during this time, they were kept in their home cage to encourage periods of sleep. The mice did not have previous training on the linear track, so on the first recording day, it was initially a novel environment. They did have three days of exposure prior to the first few recordings days on the open field, which was therefore a familiar environment at the time of recordings. After each recording session, the tetrodes were slightly turned down to continue pushing the tetrodes through the tissue. The mice were recorded for at least 6 days, or until the tetrodes moved past the CA1 pyramidal layer (which was recognized by the lack of SWRs and by unit clusters disappearing), whichever came first.

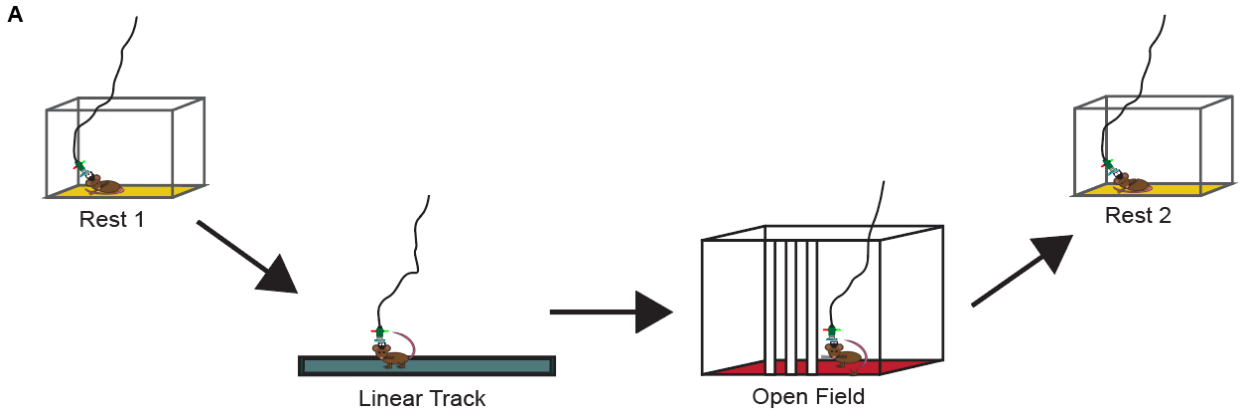

Figure 3. Schematic of Daily Recording Sessions. Each daily behavioral recording session consisted of the mice spending 10 minutes in a 'rest' phase, followed by running 10 laps on a 100cm long linear track, then exploring a 60 cm^2 open field arena for ~8 minutes. The session was concluded with another 10-minute 'rest' phase. The 'rest' phases were conducted while the mice were in their home cages, which were enclosed by a small Plexiglas box. During each phase, a cable was connected to a plug on the Microdrives to transmit electrical signals to a Neuralynx data acquisition system.

Histological Processing

Perfusion: All mice were anesthetized in a chamber that was filled with 4% isoflurane at a flow rate of 0.4 L O2/min. Once they were immobile, they were given a lethal 0.1 ml injection of sodium pentobarbital. After the breathing rate of the mice slowed to ~12 beats/min, they were perfused with cold Ringer's solution [135mM NaCl, 5.4mM KCl, 1mM MgCl2•6H2O, 1.8mM CaCl2•2H2O, 5mM HEPES] for 2-3 minutes. The mice were then perfused with 4% Paraformaldehyde (PFA) for 7-8 minutes. Their heads were removed from the rest of their body and set aside for 3-4 hours to allow PFA to further fix the brain tissue around the tetrodes, leaving slight lesions that helped identify the location of the tetrodes during the recordings. Then, the tetrodes were slowly turned upwards and away from the brains. The brains were carefully extracted and refrigerated in a 1x PBS solution overnight. The following day, the brains were transferred to a 30% sucrose (in 1x PBS) solution refrigerated for 2 days, or until the brains sunk.

Tissue Collection: A Leica microtome was used to section the brain tissue coronally into 40 µm thick slices. Every other brain slice was placed in 1x PBS and 0.02% Na-Azide, respectively. The slices in 1x PBS were mounted within one week after the tissue was sectioned. The slices in 0.02% Na-Azide were stored at 4° C for future immunohistochemical analysis.

Imaging: The mounted brain sections were stained with DAPI (4", 6-diamidino-2-phenylindole), cover-slipped, and left to dry for 2 days. The slides were then imaged with a confocal microscope using a 10x magnification lens. The images were then manually examined to locate the tetrodes for each animal and to ensure they were positioned in tissue with GFP expression. The exact location of the injection site was unable to be determined by imaging because the Microdrive was surgically implanted above the inject site. If the brain slices showed

lesions in the hippocampus this indicated that the hippocampus was damaged, and these animals were excluded from the dataset.

Data Analysis

GFP Expression. The number of cells expressing GFP were manually counted in a 0.375 mm^2 ROI (Region of Interest) for each experimental group. The ROIs were created through ImageJ (Schindelin et al., 2012). Four ROIs were created per mouse, with each surrounding one of the four tetrodes that were implanted and passed through the CA1 pyramidal layer. The number of cells per mm^2 for the control, Cox6a1 KD, and Cox6a2 KD groups were quantified.

Spike Sorting. Manual clustering of the spikes was done through MClust, MATLAB 2009b customized by Mankin et al. The clustering was performed using two-dimensional projections with waveform amplitude, waveform energy, and peak-to-valley ratio as parameters. The cells were tracked for stability across each phase of the recording session and accepted for further data analysis if they took up the same region of cluster space from rest 1 to rest 2, without overlapping with the cluster of another cell. Once all the spikes were assigned to clusters that were separated from other clusters, the spike waveform, auto-correlogram, and peak plot of each cell were examined manually to exclude clusters with noise signals.

Cell Classification. Once the spikes were sorted into clusters, the units were differentiated and classified as 'putative principal cells' and 'putative interneurons.' For each unit/cluster the average waveform of action potentials was inverted resulting in an early upward peak (peak) and a later downward peak (valley). A peak-valley ratio was then calculated by dividing the absolute amplitude of peak by the absolute amplitude of the valley. The amplitude of the first peak is related to the rise time of the depolarization, while the amplitude of the valley is related to the decay time

of repolarization (Henze et al., 2000). Spike ratios are closer to the value of 1 for interneurons, which have comparable rates of depolarization and repolarization. Next, each unit was plotted on a graph showing the value of the peak-to-valley ratios (x-axis) against average firing rate (Hz) (y-axis) during 'open field' phase for the control, Cox6a1 KD, and Cox6a2 KD groups. To compare the distributions of the units across the groups, each graph was separated into quadrants by two lines: a horizontal line where the average firing rate was 5 Hz, and a vertical line where the peak-to-valley ratio was 1.5. Quadrant 1 was on the top left (below 1.5 on the x-axis, above 5 Hz on the y-axis), Quadrant 2 was on the top right (above 1.5 on the x-axis, above 5 Hz on the y-axis), Quadrant 3 was on the bottom left (below 1.5 on the x-axis, below 5 Hz on the y-axis), and Quadrant 4 on the bottom right (above 1.5 on the x-axis, below 5 Hz on the y-axis). The quadrants were assigned based on the unit distributions of the control group, where quadrant 1 held a large density of units similar to what is expected for classical interneurons, and quadrant 4 held a large density of units similar to what is expected for classical principal cells. Thus, quadrant 1 was used to classify the cells as 'putative classical interneurons (INTs)' and quadrant 4 was used to classify the cells as 'putative classical principal cells (PCs).' Quadrant 2 was used to classify cells with a high firing rate and broad peak-to-valley ratio as 'high firing rate/broad waveform cells' (HFR/BWs). Quadrant 3 were likely pyramidal cells with atypical waveforms, but to use conservative criteria for the identification of putative pyramidal cells, it was excluded from the analysis.

Once the spikes were assigned to cell groups, a speed score was calculated for PCs and HFR/BWs. To calculate the speed score, first the instantaneous firing rate was calculated for each of the spikes that occurred when each mouse running at a velocity above 2cm/sec. Then, a Pearson correlation coefficient was calculated between the instantaneous firing rate and instantaneous

velocity, and that value was used as the speed score for each cell. Also, a bursting index was calculated for the PCs and HFR/BWs by taking the total number of spikes occurring in bursts and dividing them by the total number of spikes.

The spatial firing patterns of each cell group were examined for place fields by processing the data of each recording session with MATLAB scripts. Within the putative classical principal cells group, all cells that had at least one place field during the 'open field' phase were identified as place cells. Place fields were classified according to the following criteria: (1) the peak firing rate of the cell was at least 3 Hz in one spatial bin (bin size: 2.5 cm^2), (2) the field was comprised of bins in which the firing rate was >30% of the peak firing rate, and (3) the minimum number of bins > 30 % of peak rate was 8.

Statistics: GraphPad Prism 8.4 was used for all statistical analyses. In all instances where the Cox KD groups were compared to the control group, a Kruskal-Wallis statistical test was performed. This test was chosen because it is a non-parametric test and because a normal distribution of the data could not be assumed. A post hoc Dunn's multiple comparisons test was performed between control and Cox6a1 groups and between control and Cox6a2. The results of the tests are described in detail in Chapter II: Results.

CHAPTER II: RESULTS

Histological Analysis Confirmed GFP Expression of Viral Vectors and Tetrode Location

Cre-dependent viral constructs were injected into the hippocampal CA1 area of PV-Cre mice, and their expression was examined by imaging brain slices. The constructs used for the Cox6a1 KD and Cox6a2 KD groups co-expressed GFP (green fluorescent protein) with either Cox6a1 or Cox6a2 shRNA (short hairpin RNA), respectively. The co-expression allowed imaging of GFP to indicate shRNA expression. The control group was injected with AAVDJ-EF1α-DIO-EmGFP, the Cox6a1 KD group was injected with AAVDJ-EF1α-DIO-EmGFP-miRNA165-Cox6a1, and the Cox6a2 group was injected with AAVDJ-EF1α-DIO-EmGFP-miRNA254-Cox6a2 (Figure 4a). In addition, brain slices were also stained with DAPI (4", 6-diamidino-2-phenylindole) to show the cell layers (Figure 4a and b). We examined the images to confirm the injection of the viral constructs was located in the CA1 region of the hippocampus, which was indicated by the presence of GFP (Figure 4b). Expression of GFP was also found in the cortex and in the CA3 region of the hippocampus, which is consistent with the injection tract and the presence of PV+ interneurons in these regions. While it is expected to find PV+ interneurons outside of the CA1 layer, the leakage of the viral construct to surrounding regions was not an issue in our study, because the data we collected was locally recorded from CA1. In a separate subset of PV-Cre mice, immunohistochemical analysis confirmed GFP expression was selectively targeted to PV+ interneurons (data not shown). This further supports that the GFP expression from the viral construct is a reliable proxy for identifying PV+ interneurons in PV-Cre mice.

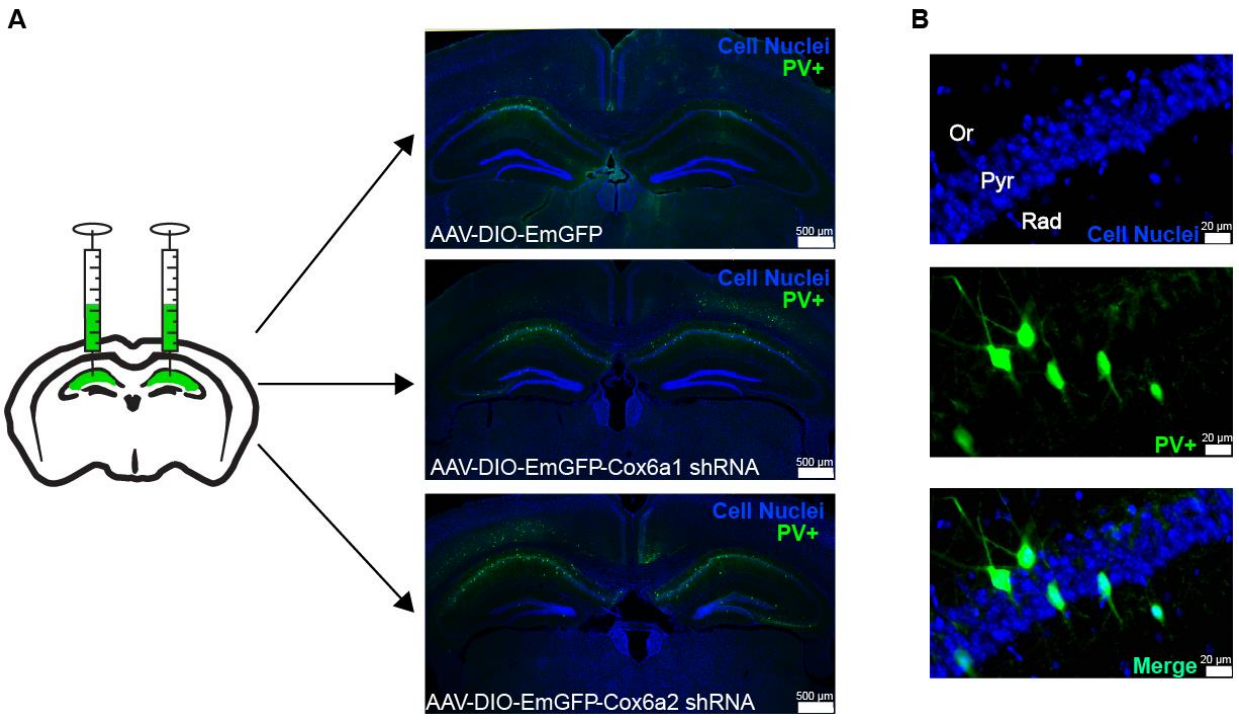

Figure 4 Histological analysis confirmed that AAV constructs resulted in GFP expression in putative PV+ neurons in the CA1 region of PV-cre mice. (A) Bilateral injections of a viral vector solution (0.5 µl per hemisphere) were targeted at the hippocampal CA1 region. The control group was injected with AAVDJ-EF1α-DIO-EmGFP (top), the Cox6a1 KD group was injected with AAVDJ-EF1α-DIO-EmGFP-miRNA165-Cox6a1 (middle) and the Cox6a2 group was injected with AAVDJ-EF1α-DIO-EmGFP-miRNA254-Cox6a2 (bottom). DAPI (blue) was used to stain cell nuclei while the constructs resulted in GFP (green) expression selectively in putative PV+ interneurons. Scale bar, 500 µm. (B) In the CA1 region, GFP expression labeled putative PV+ interneurons within the pyramidal layer. (Or,stratum oriens; Pyr, stratum pyramidale; Rad, stratum radiatum). Scale bar, 20 µm.

After expression of the viral construct was confirmed to occur within putative PV+ interneurons by visualizing the GFP expression, we located the tetrodes on the brain images, and ensured they were in the CA1 region of the hippocampus (Figure 5a). While examining the images, we found lesions around the recording tetrodes in 12 of the 30 animals that we recorded from and excluded those animals from the dataset despite expression of GFP (Figure 5b). This was to exclude the possibility of our data being altered by the damaged hippocampal area, so only data

from intact hippocampal regions were used. Once the tetrodes locations were confirmed to be in CA1 in the intact brains, we quantified the number of cells that expressed GFP around the tetrodes by creating 0.375 mm^2 ROI (regions of interest – a rectangle of 500 by 750 μm) that surrounded each of the four tetrodes (Figure 5c). The number of cells with GFP expression per mm^2 was plotted for the control, Cox6a1 KD, and Cox6a2 KD groups (Figure 5d). There was no difference in density of expression between the control and Cox6a1 group, or the control and Cox6a2 KD group (Kruskal-Wallis [KW] test, control v. Cox6a1 $p=0.2115$, control v. Cox6a2 $p=0.1366$). Also, the Cox6a1 KD group did not have a difference in the density of expression compared to the Cox6a2 KD group (KW test, $p>0.9999$). Thus, we determined the extent of GFP expression was similar across all groups, which indicated there was similar expression of the viral vector around the recording sites between the Cox6a1 KD group and Cox6a2 KD group with the control group.

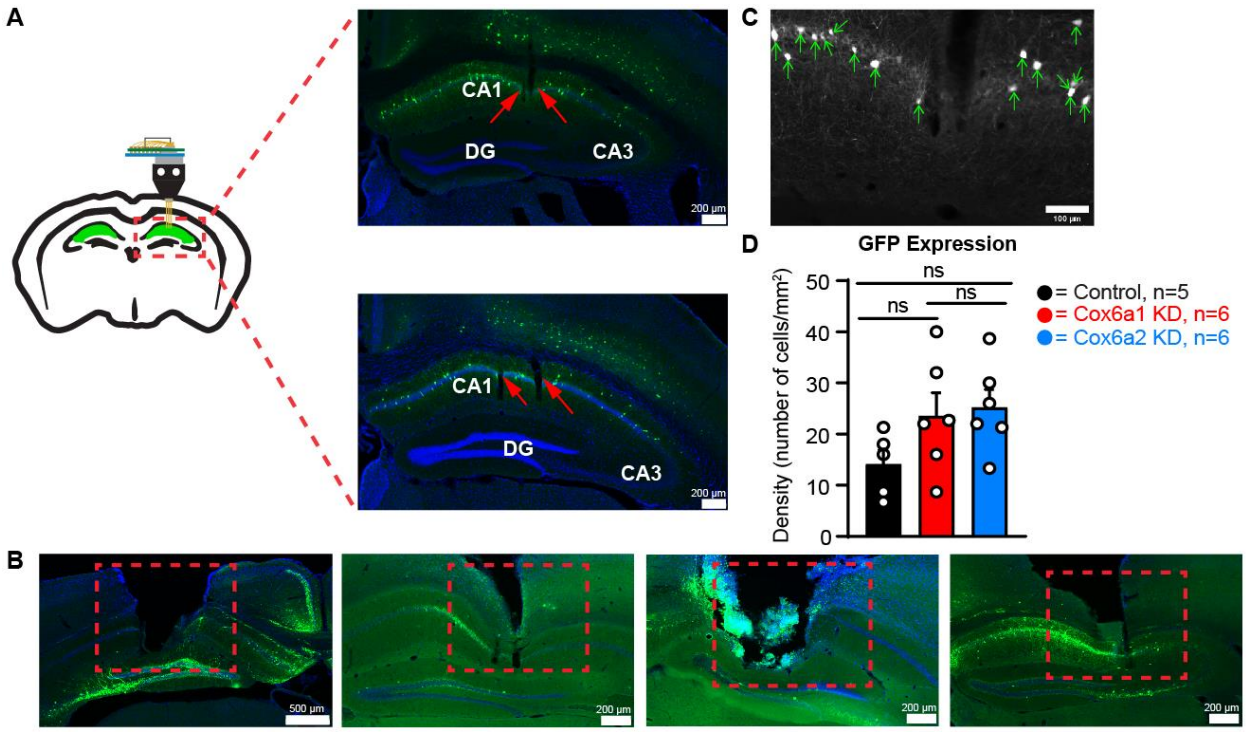

Figure 5. Histological analysis confirmed that the tetrodes were localized within the CA1 region of the hippocampus. (A) Schematic showing that the electrodes of the microdrive were placed in the CA1 region of the hippocampus. Histological analysis confirmed the location of the recording sites to be in CA1, within the region of the GFP expression. DAPI is in blue, and GFP is in green. Scale bar, 200 µm. (B) Example sections from animals that were removed from the dataset due to hippocampal lesions around the tetrodes. DAPI is in blue and GFP is in green. Scale bar, 200 µm except for image on the left, 500 µm. (C) A 0.375 mm2 region of interest (ROI) was used to quantify the number of cells (green arrows) with GFP expression (in white) around the recording tetrodes. Scale bar, 100 µm. (D) There was no difference in the density of cells (mean number of cells per mm2 ± SEM) expressing GFP in each group (Kruskal-Wallis [KW] test, $p > 0.05$).

Reduction of Cox6a2 Decreased the Peak Firing Rate of Putative Principal Cells

After GFP expression was analyzed around the recording sites, we analyzed the single-unit spiking activity from the CA1 region. Only spike waveforms obtained from recordings during the 'open field' phase of each recording session. The number of animals was consistent across all experimental groups (control n=6, Cox6a1 KD n=6, Cox6a2 KD n=6). Using the criteria outlined in Chapter 1: Methods, the spikes were first sorted into quadrants based on average firing rate

(lower or higher than 5 Hz) and peak-to-valley ratio of the spike waveform (lower or higher than 1.5) taken from recordings during the 'open field' phase of each recording session. Informed by the relationship between peak-valley ratio and average firing rate in control mice we defined four distinct quadrants (Figure 6a). Most of the cells in the control group were included in two quadrants, which we considered "putative interneurons" (INTs, quadrant 1, Q1) and "putative principal cells" (PCs, quadrant 4, Q4) (Figure 6a). Most cells in the KD groups also had characteristics of INTs and PCs and were classified accordingly. In addition, KD groups also had more cells than controls with an atypical combination of high firing rates and broad waveforms (HFR/BWs, quadrant 2, Q2) (Figures 6b, 6c, and 6d). The proportion of cells within each cell group was compared across the different manipulations (Figure 6d). Both KD groups had a difference in the distribution of cell types compared to the control group (Chi-Square test, control v. Cox6a1 KD $p=0.0003$, control v. Cox6a2 KD $p=0.0007$) (Figure 6d). This is most likely caused by the increased proportion of HFR/BW cells in both of the KD groups compared to the controls. Between the KD groups themselves, the Cox6a1 KD group did not have a difference in the distribution of cell types compared to the Cox6a2 group (Chi-Square test, $p=0.3595$). Units found in the third quadrant (Q3) had characteristics similar to principal cells but were excluded keep a conservative criterion of defining principal cells and interneurons. For the remaining three quadrants, the firing characteristics of cells in each category (INT, PC, HFR/BW) were compared between the control group and the Cox6a1 and Cox6a2 KD groups.

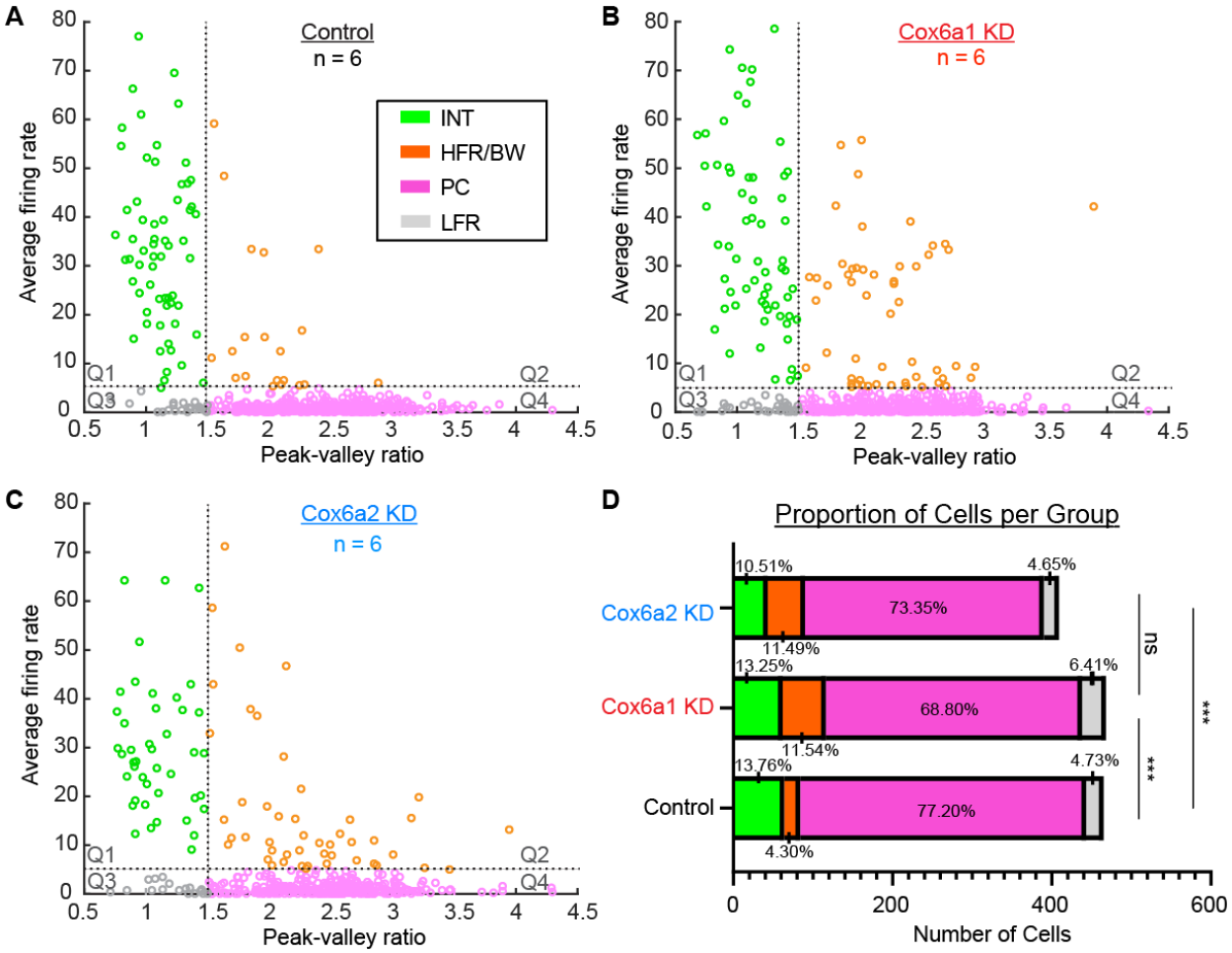

Figure 6. Spikes were classified as different cell types based on their firing characteristics. (A-C) The average spike waveform for each individual cluster was plotted as a scatterplot of the peak-to-valley ratio along the x-axis against the average firing rate (AFR, in Hz) along the y-axis. Each graph was separated into four quadrants by a horizontal line where the AFR was 5 Hz and a vertical line where the peak-to-valley ratio was 1.5. Spikes were classified into cell types per each quadrant: Quadrant 1 (Q1), putative interneurons (INTs); Q2 high firing rate/broad wavelength (HFR/BWs); Q3 principal cells (PCs); and Q4 low firing rate (LFR). (D) There was a significant difference in the distribution of cell types in the KD groups compared to the controls. Chi-square (and Fischer exact) test; $p > 0.05$, ***$p < 0.001$.

During periods of running in the open field (velocity above 2 cm/s), the mean and peak firing rates of INTs did not show any differences between the control and the Cox6a1 KD group (KW test; mean $p>0.9999$, peak $p>0.9999$ (Figure 7a). When comparing the control group to the Cox6a2 KD group, there were similarly no differences in the mean and peak firing rates (KW test;

mean p=0.4461, peak p=0.2098). There was also no difference in the mean and peak firing rates between the Cox6a1 KD and Cox6a2 KD groups (KW test; mean p=0.4251, peak p=0.0743). Since interneurons are thought to be speed modulated, the speed scores for the INTs was calculated between each group. There was no difference in the speed score of interneurons when the control group was compared to either of the KD groups, or between the KD groups compared to each other (KW test, control v. Cox6a1 KD p>0.9999, control v. Cox6a2 KD p>0.9999, Cox6a1 KD v. Cox6a2 KD p>0.9999).

Similar to the INTs, the mean and peak firing rates of PCs did not differ between the control group and Cox6a1 KD groups (KW test; mean p>0.9999, peak p=0.4301) (Figure 7b). The mean firing rate also did not differ when the Cox6a2 KD group was compared to the control group or the Cox6a1 KD group (KW test, control v. Cox6a2 KD p>0.9999, Cox6a1 KD v. Cox6a2 KD p>0.9999). In contrast to the INTs, there was a decrease in peak firing rate for the Cox6a2 KD group when compared to the control group and the Cox6a1 KD group (KW test, control v. Cox6a2 KD p<0.0001, Cox6a1 KD v. Cox6a2 KD p<0.0001). To better evaluate the firing capacity of cells during of periods of high firing we evaluated the busting index of PCs. While the burst index of PCs was not different between the control group and the Cox6a1 KD group, there was a decrease in the burst index for the Cox6a2 KD compared to the control group (KW test, control v. Cox6a1 KD p=0.0525, control v. Cox6a2 KD p<0.0001). The Cox6a2 KD group also had a decreased burst index when compared to the Cox6a1 KD group (KW test, p=0.0134). Overall, these data indicate that Cox6a2 has a more pronounced role than Cox6a1 in regulating interneuron firing rates and has a stronger influence on the firing rate of other neurons within the CA1 region.

Finally, as seen in the INTs and the PCs groups, the mean and peak firing rates of HFR/BWs were not different between the control group and Cox6a1 KD group (KW test; mean

p>0.9999, peak p>0.9999) (Figure 7c). Similar to the INTs, was no difference in the mean or peak firing rates for the Cox6a2 KD group when compared to the control group either (KW test; mean p>0.9999, peak p>0.9999). There was also no difference in either the mean or the peak firing rates when the Cox6a1 KD group was compared to the Cox6a2 KD group (KW test; mean p>0.9999, peak p=0.2508). Also similar to the INTs, there was no difference in speed score for the HFR/BWs, when the control group was compared to either of the KD groups, nor when the KD groups were compared to each other (KW test; control v. Cox6a1 KD p>0.9999, control v. Cox6a2 KD p>0.9999, Cox6a1 KD v. Cox6a2 KD p>0.9999). There was no difference in the burst index for HFR/BWs when the control group was compared to either of the KD groups, nor when the KD groups were compared to each other (KW test; control v. Cox6a1 KD p>0.9999, control v. Cox6a2 KD p>0.9999, Cox6a1 KD v. Cox6a2 KD p=0.1891).

It is also important to note that there were fewer animals reported in the control group for the HFR/BW cells (control n=4, Cox6a1 KD n=6, Cox6a2 KD n=6) while the number of animals stayed consistent throughout each experimental group for PCs (control n=6, Cox6a1 KD n=6, Cox6a2 KD n=6) and INTs (control n=6, Cox6a1 KD n=6, Cox6a2 KD n=6). This is because two of the control animals did not have any cells in Q2 that could be classified as HFR/BW, emphasizing the uniqueness of the HFR/BW cells to the Cox KD manipulation.

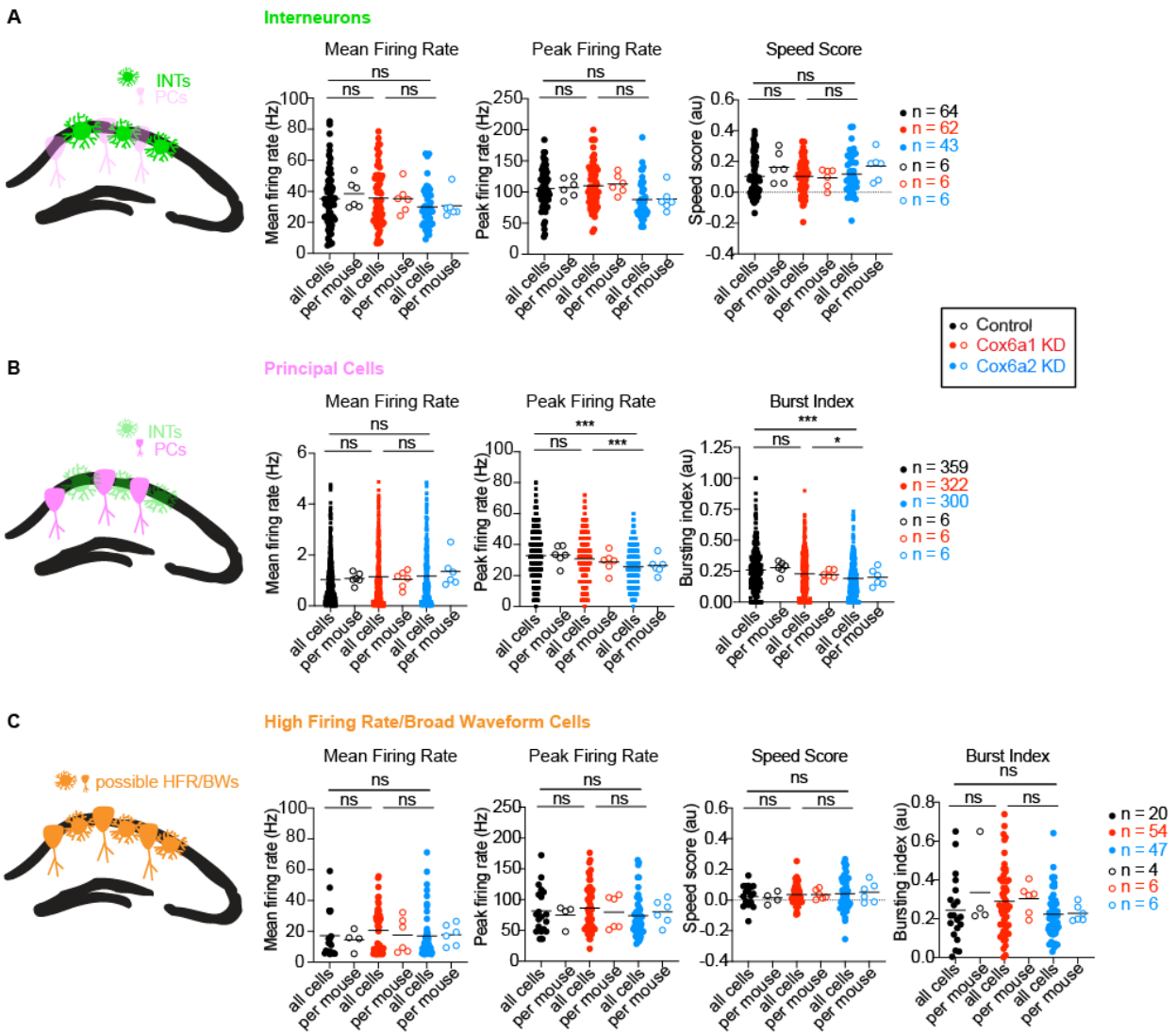

Figure 7. Single-unit recording data from the CA1 region revealed that the peak firing rate for putative interneurons was decreased when Cox6a2 was knocked-down. (A) Putative interneurons (Is) are depicted in green in the schematic to the left. For interneurons, there were no differences for any of the measurements between the control group and the KD groups, as well as between the KD groups themselves. (B) Putative principal cells (PCs) are depicted in pink on the schematic to the left. For PCs, there was a decrease in the peak firing rate and burst index for PCs when the Cox6a2 KD group was compared to control group and the Cox6a1 KD group. (C) High firing rate/broad waveform cells (HFR/BWs) are depicted in orange in the schematic to the left. There were no differences between any of the groups across the measurements for HFR/BWs. For all panels, ***$p < 0.001$, **$p < 0.01$, KW test followed by Dunn's multiple comparisons test. Each black line indicates the mean. Closed circles indicate all data points per cell, open circles indicate averaged data per mouse. The control group is shown in black, the Cox6a1 KD group is shown in red, and the Cox6a2 KD group is shown in blue.

Cox6a1 KD and Cox6a2 KD Increased the Size of Place Fields in CA1

Analysis of the spatial firing patterns of PCs allowed us to identify place cells and analyze their place fields through the criteria provided in Chapter I: Methods (Figure 8a). The number of cells per group used in the analyses were: control n=274, Cox6a1 KD n=215, Cox6a2 KD n=191. To analyze the differences in place field properties between the two KD and control groups, we began by measuring the number of place fields per cell (Figure 8b). The Cox6a1 and Cox6a2 KD groups had an increased number of place fields compared to the control group (KW test; control v. Cox6a1 $p=0.0078$, control v. Cox6a2 $p=0.0036$). When the Cox6a1 KD group was compared to the Cox6a2 KD group, did not have a difference in the number of place fields (KW test; $p>0.9999$). Next, we compared the size of the place fields (Figure 8c). The Cox6a1 KD and Cox6a2 KD groups both had place fields that were significantly larger than those in the control group (KW test; control v. Cox6a1 $p=0.0007$, control v. Cox6a2 $p<0.0001$). The Cox6a2 KD group also showed an increase in place field size when compared to the Cox6a1 KD group (KW test; $p=0.0160$) The increase in place field number and size for both Cox6a1 and Cox6a2 KD groups suggest that the mitochondrial subunits play an important role in regulating how spatial information is encoded in the hippocampus.

To measure the precision of spatial firing without having to define place fields, we also quantified the spatial information in bits/spike and in bits/second (Figure 8d-e). Here we observed that the spatial information decreased for the Cox6a2 KD group when compared to the control group (KW test, $p<0.0001$ bits/spike; $p=0.0075$ bits/second) (Figure 8d and Figure 8e). The decrease in spatial information is consistent with the increase in place field size, as broader fields are expected to have less information about spatial location. The Cox6a1 KD group also showed a decrease in information in bits per spike, but no difference in bits per second compared to the

control (KW test, p=0.0002 bits/spike; p>0.9999 bits/sec). We also observed a decrease in the spatial information in the Cox6a2 KD group when compared to the Cox6a1 KD group (KW test, p=0.0008 bits/spike; p=0.0021 bits/second).

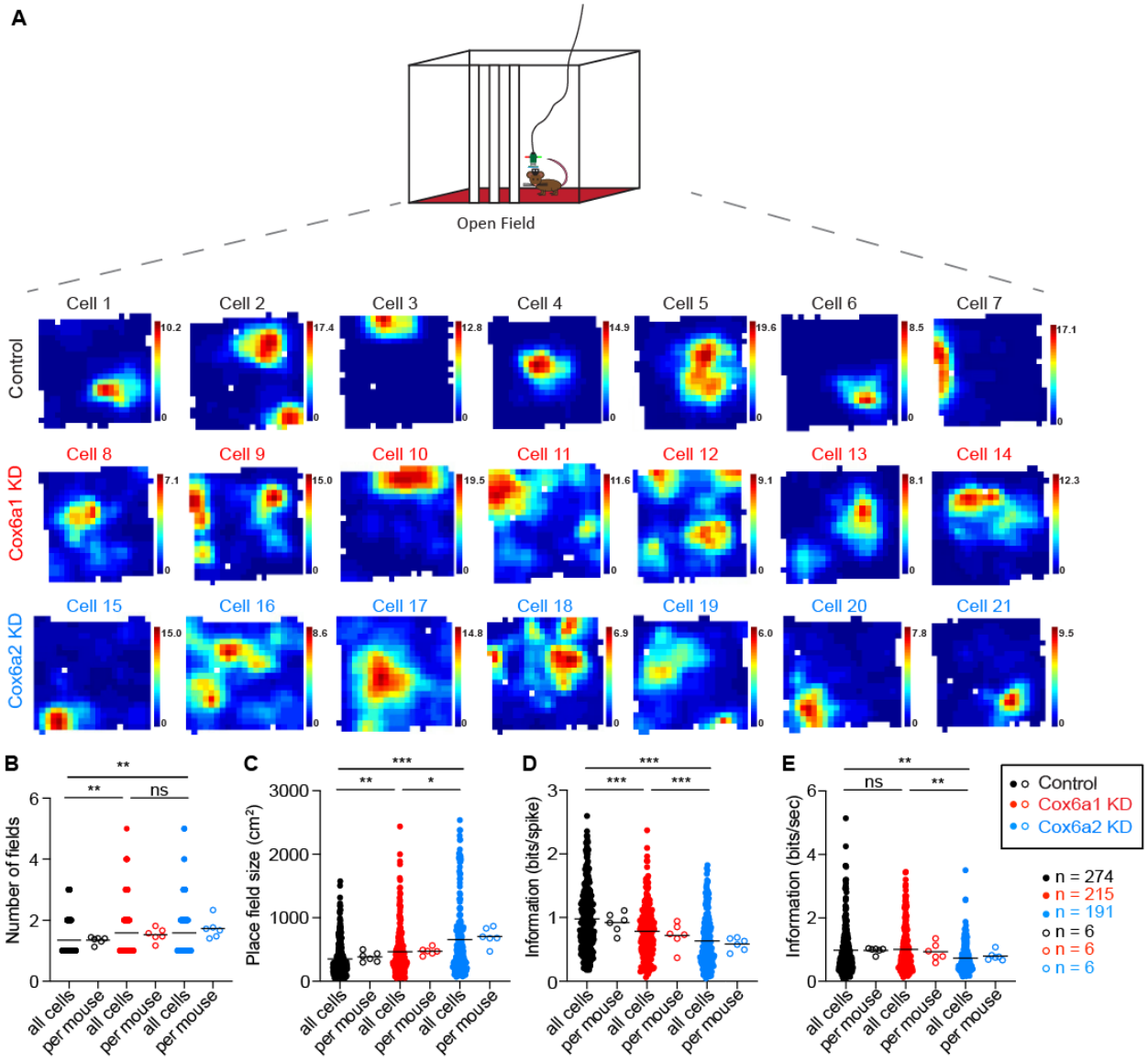

Figure 8. Knocking down Cox6a1 and Cox6a2 increased the place field size of principal cells in the CA1 region. (A) The mice spent ~8 minutes exploring an open field environment. For recordings in the open field, heat maps displaying the place fields of place cells were generated for the control, Cox6a1 KD, and Cox6a2 KD groups. The displayed cells are taken from different recording days and from different animals. (B) The number of place fields per cell were increased for both KD groups compared to the control group. (C) The place field sizes were also increased for both KD groups compared to the control group, as well as for the KD groups compared to each other. (D) Information (bits/spike) decreased for both KD groups when compared to controls, as well as when compared to each other, and (E) information (bits/sec) decreased for the Cox6a2 KD group compared to the control group and the Cox6a1 KD group. All statistical comparisons were performed with a KW test followed by Dunn's multiple comparison test, ***$p < 0.001$, **$p < 0.01$, *$p < 0.05$. Each closed circle is a cell, and black lines indicate the mean over all cells in a group. Each open circle is the data averaged per mouse in each group, and the corresponding black lines indicate the mean over all mice.

Cox6a2 decreased frequency of theta and gamma oscillations

We also performed an analysis of the local field potential (LFP) recorded from the CA1 region. The data from the Cox6a1 KD and Cox6a2 KD groups was compared to the control group. LFP analysis revealed that there was no difference between the Cox6a1 group and the control group in the frequency of theta or gamma rhythms (KW test; theta $p>0.9999$, gamma $p>0.9999$) (theta, Figure 9a; gamma, Figure 9b). On the other hand, there was a significant decrease in the Cox6a2 KD group when compared to the control group in both the theta and gamma frequency (KW test, theta $p=0.0178$ gamma $p=0.0057$). Compared to the Cox6a1 KD group, the Cox6a2 KD did not a difference in theta frequency but did have a decrease in gamma frequency (KW test, theta $p=0.1439$; gamma $p=0.0053$). These data suggest Cox6a2 plays a role in regulating the frequency of theta and gamma, while Cox6a1 does not. It is important to note that gamma oscillations were not detected for all animals (control n=5, Cox6a1 KD n=3, Cox6a2 KD n=4), reducing the number of animals in the analysis, while theta oscillations were detected for all animals (n=6 for all). There was no difference in the abundance of sharp wave ripples (SWRs) between any of the groups (KW test, control v. Cox6a1 $p>0.9999$, control v. Cox6a2 $p>0.9999$, Cox6a1 KD v. Cox6a2 KD $p=0.9309$). This suggests that each of the mitochondrial subunits, along with the remaining lower levels of the other subunit, was sufficient for providing sufficient energy for generating these transient events (Figure 9c).

To analyze whether the effects on theta oscillations correlate with the extent of expression of our constructs, we plotted the average theta frequency against the levels of GFP expression we found in the ROIs mentioned above (Figure 9d). For the Cox6a2 KD group, we observed that an increase in the number of cells with GFP expression was related to a decrease in theta frequency.

A smaller decrease in theta frequency is observed for the Cox6a1 KD group as the number of cells with GFP expression is increased. While there is a negative relation between construct expression and frequency in both Cox KD groups, there is no apparent relation between expression and frequency in the control group. Overall, this shows the decreased theta frequency for the Cox6a2 group is correlated with the level of GFP expression.

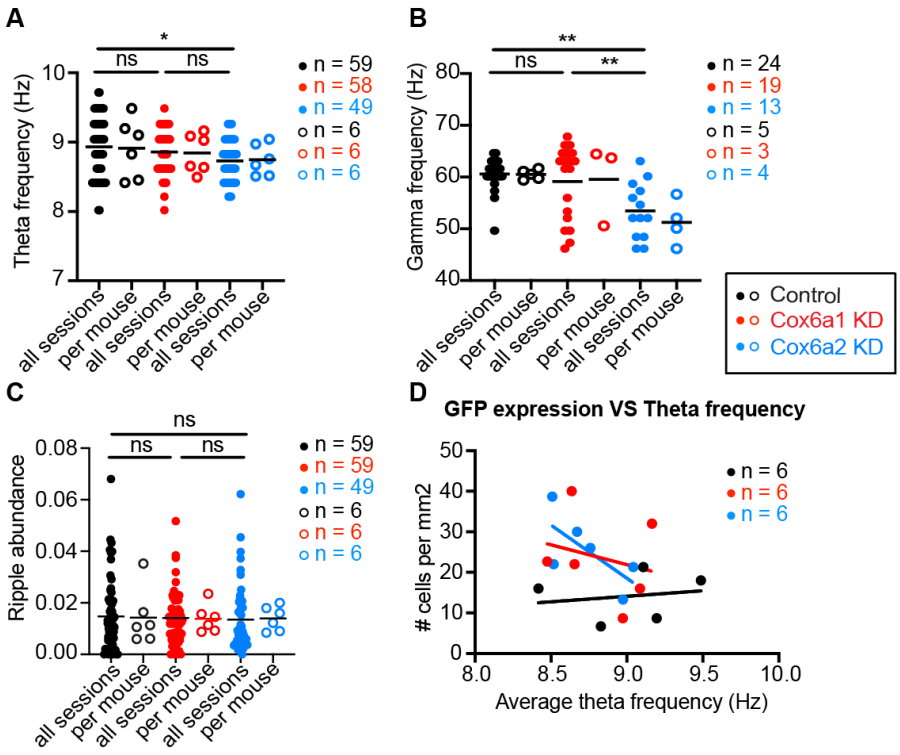

Figure 9. Reducing levels of Cox6a2 in PV+ interneurons reduced the frequency of hippocampal oscillations. (A-C) Theta frequency, gamma frequency and sharp wave-ripple (SWR) rates for the control and experimental groups are shown. Theta and gamma frequency data were taken from periods when the animal was moving at speeds > 2 cm/s. SWR rates were calculated from the occurrence of a SWR during times when the animal was resting (speed < 2 cm/s). (A) There was a decrease in theta frequency in Cox6a2 KD group compared to the control group. (B) There was a decrease in gamma frequency in the Cox6a2 KD group compared to both the control and Cox6a1 KD groups. (C) There was no difference in ripple abundance between any of the groups. All statistical comparisons were performed with a KW test followed by Dunn's multiple comparison test, **p < 0.01, *p<0.05. (D) The correlation between average theta frequency with the number of cells expressing GFP per mm^2 in the ROIs.

Chapter III: DISCUSSION

PV+ interneurons are known to have a have a larger presence of cytochrome c oxidase (complex IV of the Electron Transport Chain) than any other neuron type in the hippocampus, suggesting they are the most metabolically active neurons in the hippocampus (Gulyás et al., 2006). In this thesis, we utilized Cre-dependent viral vector constructs to express shRNAs that selectively knocked down the mitochondrial proteins, Cox6a1 and Cox6a2, within PV+ interneurons of the CA1 hippocampal region in PV-Cre mice and confirmed targeting of the shRNAs to PV+ interneurons in the vicinity of our recording sites in CA1 (Figure 4-5). As a result of knocking down Cox6a1, we observed no change in the firing rates of interneurons and PCs, an increase in size of place fields, and no change in the LFP (Figures 6-8). Knocking down Cox6a2 appears to have indirectly altered function of PCs profoundly. We observed a decrease in the peak firing rates of PCs, an increase in the size of place fields, and a decrease in theta and gamma oscillations (Figures 6-8). As we expected, we saw a larger influence on the firing properties and the LFP with the Cox6a2 KD group, which suggests the importance of Cox6a2 within the hippocampal CA1 region.

Our viral vector constructs were Cre-dependent and included GFP in addition to the shRNA. We could therefore analyze the expression of the viral constructs by visualizing the GFP expression by carrying out histological procedures. As expected for the PV-Cre mice that were used in our experiments, the pattern of cells with GFP expression matched the known distribution of PV+ interneurons in the CA1 region (Figure 4-5). Therefore, the constructs appeared to be selectively expressed in PV+ cells. In parallel experiments by the Pekkurnaz lab (V. Luczak and G. Pekkurnaz, unpublished data), the shRNA constructs were confirmed to be Cre-dependent and to knock down the levels of Cox6a1 and Cox6a2 after three weeks. Although it is known that the

turnover of proteins in mitochondria is slow, these data suggest that there was at least a partial decrease in protein levels at the time when we performed the recordings, which was ~3.5-5 weeks after viral injections. Alternate brain sections were saved for future immunohistochemistry experiments where the quantification of 1) percentage of PV+ cells infected and 2) level of protein knock-down will be performed. Meanwhile our current histological analysis confirmed that all tetrodes used for data collection terminated within the CA1 region and that all tetrodes had cells with GFP expression in the proximity. Given that we observed physiological changes in firing rates, place field size, and oscillation frequencies in the CA1 region, in particular as a result of the Cox6a2 shRNA expression, it is evident that our constructs resulted in a level of protein reduction that altered neuronal function. Further analysis will allow better characterization of our results.

Although principal cells were not directly manipulated in this study, we found altered firing patterns of PCs with the expression of the viral vector constructs (Figure 7). This effect was indirect and can be attributed to the influence of PV+ interneurons on principal cells because expression of our constructs was limited to interneurons. We show that the indirect influence from the interneurons was sufficient in causing severe effects on the PCs we recorded from. Previous studies have shown that by decreasing the firing rate of interneurons, which are known to inhibit principal cells, the firing rate of principal cells would increase by the decrease in inhibition (Stark et al., 2014). This is contrary to what we see, as INT firing rates were unchanged, while PC peak firing rate was still decreased, and the average firing rates for INTs and PCs were not altered in the Cox6a1 and Cox6a2 KDs groups. Given that our manipulations were not acute, it is therefore likely that the local network reaches a new balance in which firing rates of interneurons and principal cells were regulated in a corresponding direction.

One of the most striking effects of our manipulation is that place field sizes were dramatically increased by both Cox6a1 KD and Cox6a2 KD groups (Figure 8). These results, along with the decrease in peak firing rates of principal cells, are similar to the results found by Zhang et al. (Zhang et al., 2014). In their study, they found an increase in place field size and a decrease in peak firing rate of place cells when mice were exploring a dark environment compared to a lit environment. They also found a decrease in the spatial information in the dark, where the mice did not have any visual input, which they claim suggests less accurate place cell firing. This provides a parallel example to our results that place field rate and spatial accuracy can be altered in concert, as we also see decrease in spatial information, despite differences in our experimental designs. Zhang et al. found their results with no manipulation to the hippocampus, while we injected viral vectors to produce similar alterations in the firing patterns of place cells. Also, our data collection was limited to dimly lit environments while their data was collected from both dark and lit environments and found impairments in spatial representation in dark environments. One possibility is that our interneuron manipulation caused similar effects to the loss of visual inputs by impairing the relationship between principal cells and interneurons.

Interestingly, the KD manipulations revealed an increase in a unique group of cells that we characterized as HFR/BWs (Figure 6). We did not see a difference in the firing properties of HFR/BWs in the KD groups compared to the controls, despite the increased proportion of those cells in the KD groups (Figure 7). However, this comparison should be taken with a grain of salt because two control animals were not included in the dataset because they did not have any cells in this group, and one control animal only had 1 HFR/BW cell. It is also possible that the HFR/BWs could be principal cells as well as interneurons affected by the manipulation, creating mixed characteristics within the group. For HFR/BW cells that could be principal cells, it is also possible

that some of those cells are also place cells that were not included in the place field analysis due to our criteria requiring place cells to be classified as principal cells. A more in-depth analysis of the waveform and spiking pattern of these cells must be performed to determine the HFR/BWs indeed have altered characteristics as a result of the KD manipulation.

Previous studies have reported that PV+ interneurons are critical for generating gamma oscillations (Cardin et al., 2009; Ferguson & Gao, 2018; Gulyás et al., 2010; Sohal et al., 2009). Optogenetic inactivation of PV+ interneurons has also been shown to disrupt theta oscillations and network dynamics within CA1, which influence memory functions (Ognjanovski et al., 2018). Conversely, optogenetic activation of PV+ interneurons has been shown to play a role in restoring both theta and gamma oscillations (Chung et al., 2020). Our study adds to these reports and suggests that the high energy demand of PV+ interneurons needs to be met for PV+ interneurons to perform their role in maintaining hippocampal gamma and theta oscillations within the normal frequency band. In particular, the decrease in theta and gamma frequencies selectively when Cox6a2 is knocked down in the mitochondria of PV+ interneurons (Figure 9a-b) is consistent with a selective role of Cox6a2 in tissues that require ATP levels that are matched to energy demand.

We also find that effects of the knockdowns on neural oscillations do not extend to SWRs (Figure 9c). SWRs are intermittent, transient events, and it is possible they either require other interneuron types to regulate their function or that PV+ interneuron activity during these events does not require an equally high energy supply as during theta and gamma. Theta and gamma oscillations are oscillations that can be ongoing for long periods, and they may therefore require a more consistent and sustained regulation of energy in PV+ interneurons. Previous studies have shown that directly influencing the firing rate of PV+ interneurons by optogenetic manipulation causes impairments in SWRs (Gan et al., 2017; Schlingloff et al., 2014; Stark et al., 2014). Since

we do not directly alter the firing pattern of PV+ interneurons, it is possible that our influence on the physiology of PV+ interneurons are more subtle and not able to be detected by extracellular recordings. Our manipulation is closer to what is expected by the influence of a degenerative disease, so observing how the subtle changes in the PV+ interneuron physiology alter the hippocampal CA1 region could provide more insight into disease-related phenotypes. It is also possible the difference in our results compared to previous studies is due to differences in analyzing the SWRs, for which there are several techniques, and given the inconsistencies in identifying SWRs by using different techniques. Further work to refine SWR detection and analysis of the post-behavior session will be necessary to fully understand the effect of Cox6a1 and Cox6a2 on SWRs.

Throughout our study, we observe that knocking down Cox6a2 has more a pronounced influence on the CA1 physiology than knocking down Cox6a1. We see this with the decrease in PC peak firing rate and burst index, increase in place field size, decrease in spatial information, and decrease in gamma frequency (Figures 7-9). This could indicate that Cox6a2 has a more specialized role within the mitochondria of PV+ interneurons, which require it to be present to sustain function. This hypothesis can be supported by a study that identified a high concentration of Cox6a2 among PV+ interneurons in the hippocampus, compared to other cell types (Tasic et al., 2016), thus implying a unique demand for Cox6a2 in PV+ interneurons. While the role of Cox6a2 in neurons has not been studied, Cox6a2 has been shown to increase complex IV activity and mitochondrial ATP production in skeletal myofibers and cardiomyocytes (Nagai et al., 2017; Quintens et al., 2013). It has also been shown that Cox6a2 increases the stability of Complex IV compared to Cox6a1, further suggesting that PV+ interneurons rely more on Cox6a2 than Cox6a1 to sustain function (Cogliati et al., 2016). It is possible Cox6a2 plays a similar role in PV+

interneurons, but further studies are necessary to determine the regulation of ATP levels in neurons. Furthermore, we can currently not exclude the possibility that our constructs have off-target effects. To confirm the importance of Cox6a2 in PV+ interneurons, it will therefore be necessary to perform a rescue experiment in which a construct that restore protein levels is expressed along with the knockdown construct. If the altered hippocampal physiology reverses to the firing patterns in control mice, this strategy would affirm that the dysfunction that we observe here emerged from reduced Cox6a2 levels.

CHAPTER IV: CONCLUSION

The influence of PV+ interneurons within the hippocampus is well documented, and it is also well established that interneurons can sustain high firing rates and may thus have a higher metabolic demand. In an attempt to uncover whether energy production in PV+ interneurons is specialized to meet the high metabolic demand, we investigated the importance of the mitochondrial subunits, Cox6a1 and Cox6a2, within PV+ interneurons. First, we confirmed that we can target viral constructs that lower the expression levels of Cox6a1 and Cox6a2 to PV+ interneurons. In recordings from freely behaving mice, we then show that reducing levels of Cox6a1 increased the size of place fields and decreased the amount of spatial information represented in the CA1 region of the hippocampus. Reducing levels of Cox6a2 also increased the size of place fields and decreased the amount of spatial information represented in the CA1 region, while also decreasing the firing rates of interneurons and PCs and decreasing the frequency of theta and gamma oscillations.

Overall, our study provides evidence as to how the metabolic functions within PV+ interneurons influence the hippocampal CA1 network. The decrease in firing properties of neurons and the impairments observed in spatial representation by reducing Cox6a1 and Cox6a2 hint at possible memory deficits that have yet to be investigated. Also, our manipulations could be a way to model the metabolic deficits found in degenerative diseases, which could help provide insight on how to treat them.

This thesis is being used to prepare a submission of publication of material by Silvia Viana da Silva; Luczak, Vince; Haberl, Matthias; Shin, Sora; Lim, Byungkook; Pekkurnaz, Gulcin; Leutgeb, Stefan. The thesis author will be a co-author of the publication.

References

Albers, D. S., & Flint Beal, M. (2000). Mitochondrial dysfunction and oxidative stress in aging and neurodegenerative disease. In *Journal of Neural Transmission, Supplement* (Issue 59, pp. 133–154). Springer, Vienna. https://doi.org/10.1007/978-3-7091-6781-6_16

Anthony, G., Reimann, A., & Kadenbach, B. (1993). Tissue-specific regulation of bovine heart cytochrome-c oxidase activity by ADP via interaction with subunit VIa. *Proceedings of the National Academy of Sciences of the United States of America*, *90*(5), 1652–1656. https://doi.org/10.1073/pnas.90.5.1652

Atallah, B. V., & Scanziani, M. (2009). Instantaneous Modulation of Gamma Oscillation Frequency by Balancing Excitation with Inhibition. *Neuron*, *62*(4), 566–577. https://doi.org/10.1016/j.neuron.2009.04.027

Bartos, M., Vida, I., & Jonas, P. (2007). Synaptic mechanisms of synchronized gamma oscillations in inhibitory interneuron networks. *Nature Reviews Neuroscience*, *8*(1), 45–56. https://doi.org/10.1038/nrn2044

Bezaire, M. J., & Soltesz, I. (2013). Quantitative assessment of CA1 local circuits: Knowledge base for interneuron-pyramidal cell connectivity. *Hippocampus*, *23*(9), 751–785. https://doi.org/10.1002/hipo.22141

Broadbent, N. J., Squire, L. R., & Clark, R. E. (2004). Spatial memory, recognition memory, and the hippocampus. *Proceedings of the National Academy of Sciences of the United States of America*, *101*(40), 14515–14520. https://doi.org/10.1073/pnas.0406344101

Buzsáki, G., Kaila, K., & Raichle, M. (2007). Inhibition and Brain Work. In *Neuron* (Vol. 56, Issue 5, pp. 771–783). https://doi.org/10.1016/j.neuron.2007.11.008

Cajal, S. R. Y. (1894). The Croonian Lecture: La Fine Structure des Centres Nerveux. *Proceedings of the Royal Society of London*, *55*, 444–468. http://www.jstor.org/stable/115494

Cardin, J. A., Carlén, M., Meletis, K., Knoblich, U., Zhang, F., Deisseroth, K., Tsai, L.-H., & Moore, C. I. (2009). *Driving fast-spiking cells induces gamma rhythm and controls sensory responses*. https://doi.org/10.1038/nature08002

Chicherin, I. V., Dashinimaev, E., Baleva, M., Krasheninnikov, I., Levitskii, S., & Kamenski, P. (2019). Cytochrome c Oxidase on the Crossroads of Transcriptional Regulation and Bioenergetics. *Frontiers in Physiology*, *10*(MAY), 644. https://doi.org/10.3389/fphys.2019.00644

Chung, H., Park, K., Jang, H. J., Kohl, M. M., & Kwag, J. (2020). Dissociation of somatostatin and parvalbumin interneurons circuit dysfunctions underlying hippocampal theta and gamma oscillations impaired by amyloid β oligomers in vivo. *Brain Structure and Function*, *225*(3), 935–954. https://doi.org/10.1007/s00429-020-02044-3

Cobb, S. R., Buhl, E. H., Halasy, K., Paulsen, O., & Somogyi, P. (1995). Synchronization of neuronal activity in hippocampus by individual GABAergic interneurons. *Nature*, *378*(2), 75–78.

Cogliati, S., Calvo, E., Loureiro, M., Guaras, A. M., Nieto-Arellano, R., Garcia-Poyatos, C., Ezkurdia, I., Mercader, N., Vázquez, J., & Antonio Enriquez, J. (2016). *Mechanism of super-assembly of respiratory complexes III and IV*. https://doi.org/10.1038/nature20157

Colgin, L. L. (2016). Rhythms of the hippocampal network. In *Nature Reviews Neuroscience* (Vol. 17, Issue 4, pp. 239–249). Nature Publishing Group. https://doi.org/10.1038/nrn.2016.21

Denis, M. (1986). Structure and function of cytochrome-c oxidase. *Biochimie*, *68*(3), 459–470. https://doi.org/10.1016/S0300-9084(86)80013-X

Deshmukh, S. S., & Knierim, J. J. (2012). Hippocampus. *Wiley Interdisciplinary Reviews: Cognitive Science*, *3*(2), 231–251. https://doi.org/10.1002/wcs.1164

Ferguson, B. R., & Gao, W. J. (2018). Pv interneurons: critical regulators of E/I balance for prefrontal cortex-dependent behavior and psychiatric disorders. In *Frontiers in Neural Circuits* (Vol. 12, p. 37). Frontiers Media S.A. https://doi.org/10.3389/fncir.2018.00037

Fries, P., Nikolić, D., & Singer, W. (2007). The gamma cycle. *Trends in Neurosciences*, *30*(7), 309–316. https://doi.org/10.1016/j.tins.2007.05.005

Gan, J., Weng, S. ming, Pernía-Andrade, A. J., Csicsvari, J., & Jonas, P. (2017). Phase-Locked Inhibition, but Not Excitation, Underlies Hippocampal Ripple Oscillations in Awake Mice In Vivo. *Neuron*, *93*(2), 308–314. https://doi.org/10.1016/j.neuron.2016.12.018

Golgi, C. (1906). *The neuron doctrine - theory and facts*.

Gulyás, A. I., Buzsáki, G., Freund, T. F., & Hirase, H. (2006). Populations of hippocampal inhibitory neurons express different levels of cytochrome c. *European Journal of Neuroscience*, *23*(10), 2581–2594. https://doi.org/10.1111/j.1460-9568.2006.04814.x

Gulyás, A. I., Szabó, G. G., Ulbert, I., Holderith, N., Monyer, H., Erdélyi, F., Szabó, G., Freund, T. F., & Hájos, N. (2010). Parvalbumin-containing fast-spiking basket cells generate the field potential oscillations induced by cholinergic receptor activation in the hippocampus. *Journal of Neuroscience*, *30*(45), 15134–15145. https://doi.org/10.1523/JNEUROSCI.4104-10.2010

Hartley, T., Lever, C., Burgess, N., & O'Keefe, J. (2014). Space in the brain: How the hippocampal formation supports spatial cognition. *Philosophical Transactions of the Royal Society B: Biological Sciences*, *369*(1635). https://doi.org/10.1098/rstb.2012.0510

Henze, D. A., Borhegyi, Z., Csicsvari, J., Mamiya, A., Harris, K. D., & Buzsáki, G. (2000). Intracellular features predicted by extracellular recordings in the hippocampus in vivo. *Journal of Neurophysiology*, *84*(1), 390–400. https://doi.org/10.1152/jn.2000.84.1.390

Hu, H., Gan, J., & Jonas, P. (2014). Fast-spiking, parvalbumin+ GABAergic interneurons: From cellular design to microcircuit function. *Science*, *345*(6196). https://doi.org/10.1126/science.1255263

Kadenbach, B., Barth, J., Akgün, R., Freund, R., Linder, D., & Possekel, S. (1995). Regulation of mitochondrial energy generation in health and disease. *BBA - Molecular Basis of Disease*, *1271*(1), 103–109. https://doi.org/10.1016/0925-4439(95)00016-W

Kann, O., Huchzermeyer, C., Kovács, R., Wirtz, S., & Schuelke, M. (2011). Gamma oscillations in the hippocampus require high complex i gene expression and strong functional performance of mitochondria. *Brain*, *134*(2), 345–358. https://doi.org/10.1093/brain/awq333

Klausberger, T., & Somogyi, P. (2008). Neuronal diversity and temporal dynamics: The unity of hippocampal circuit operations. *Science*, *321*(5885), 53–57. https://doi.org/10.1126/science.1149381

Li, Y., Park, J. S., Deng, J. H., & Bai, Y. (2006). Cytochrome c oxidase subunit IV is essential for assembly and respiratory function of the enzyme complex. *Journal of Bioenergetics and Biomembranes*, *38*(5–6), 283–291. https://doi.org/10.1007/s10863-006-9052-z

McBain, C. J. (2001). Interneurons unbound. *Nature Reviews Neuroscience*, *2*(1), 11–23. https://doi.org/10.1038/35049047

Moser, E. I. (2003). Neurobiology: Interneurons take charge. In *Nature* (Vol. 421, Issue 6925, pp. 797–799). https://doi.org/10.1038/421797a

Nagai, H., Satomi, T., Abiru, A., Miyamoto, K., Nagasawa, K., Maruyama, M., Yamamoto, S., Kikuchi, K., Fuse, H., Noda, M., & Tsujihata, Y. (2017). Antihypertrophic Effects of Small Molecules that Maintain Mitochondrial ATP Levels Under Hypoxia. *EBioMedicine*, *24*, 147–158. https://doi.org/10.1016/j.ebiom.2017.09.022

Ognjanovski, N., Broussard, C., Zochowski, M., & Aton, S. J. (2018). Hippocampal Network Oscillations Rescue Memory Consolidation Deficits Caused by Sleep Loss. *Cerebral Cortex*, *28*, 3711–3723. https://doi.org/10.1093/cercor/bhy174

Power, J. D., Fair, D. A., Schlaggar, B. L., & Petersen, S. E. (2010). The Development of Human Functional Brain Networks. In *Neuron* (Vol. 67, Issue 5, pp. 735–748). NIH Public Access. https://doi.org/10.1016/j.neuron.2010.08.017

Prestigio, C., Ferrante, D., Valente, P., Casagrande, S., Albanesi, E., Yanagawa, Y., Benfenati, F., & Baldelli, P. (2019). Spike-Related Electrophysiological Identification of Cultured Hippocampal Excitatory and Inhibitory Neurons. *Molecular Neurobiology*, *56*(9), 6276–6292. https://doi.org/10.1007/s12035-019-1506-5

Quintens, R., Singh, S., Lemaire, K., de Bock, K., Granvik, M., Schraenen, A., Vroegrijk, I. O. C. M., Costa, V., van Noten, P., Lambrechts, D., Lehnert, S., van Lommel, L., Thorrez, L., de Faudeur, G., Romijn, J. A., Shelton, J. M., Scorrano, L., Lijnen, H. R., Voshol, P. J., Carmeliet, P., Mammen, P., Puthenveetil, A., & Schuit, F. (2013). Mice Deficient in the Respiratory Chain Gene Cox6a2 Are Protected against High-Fat Diet-Induced Obesity and Insulin Resistance. *PLoS ONE*, *8*(2). https://doi.org/10.1371/journal.pone.0056719

Schindelin, J., Arganda-Carreras, I., Frise, E., Kaynig, V., Longair, M., Pietzsch, T., Preibisch, S., Rueden, C., Saalfeld, S., Schmid, B., Tinevez, J. Y., White, D. J., Hartenstein, V., Eliceiri, K., Tomancak, P., & Cardona, A. (2012). Fiji: An open-source platform for biological-image analysis. In *Nature Methods* (Vol. 9, Issue 7, pp. 676–682). Nature Publishing Group. https://doi.org/10.1038/nmeth.2019

Schlingloff, D., Káli, S., Freund, T. F., Hájos, N., & Gulyás, A. I. (2014). Mechanisms of sharp

wave initiation and ripple generation. *Journal of Neuroscience*, *34*(34), 11385–11398. https://doi.org/10.1523/JNEUROSCI.0867-14.2014

Sohal, V. S., Zhang, F., Yizhar, O., & Deisseroth, K. (2009). Parvalbumin neurons and gamma rhythms enhance cortical circuit performance. *Nature*, *459*, 698–702. https://doi.org/10.1038/jid.2014.371

Sporns, O., Tononi, G., & Kötter, R. (2005). The human connectome: A structural description of the human brain. In *PLoS Computational Biology* (Vol. 1, Issue 4, pp. 0245–0251). Public Library of Science. https://doi.org/10.1371/journal.pcbi.0010042

Stark, E., Roux, L., Eichler, R., Senzai, Y., Royer, S., & Buzsáki, G. (2014). Pyramidal cell-interneuron interactions underlie hippocampal ripple oscillations. *Neuron*. https://doi.org/10.1016/j.neuron.2014.06.023

Steullet, P., Cabungcal, J. H., Coyle, J., Didriksen, M., Gill, K., Grace, A. A., Hensch, T. K., Lamantia, A. S., Lindemann, L., Maynard, T. M., Meyer, U., Morishita, H., O'Donnell, P., Puhl, M., Cuenod, M., & Do, K. Q. (2017). Oxidative stress-driven parvalbumin interneuron impairment as a common mechanism in models of schizophrenia. In *Molecular Psychiatry* (Vol. 22, Issue 7, pp. 936–943). Nature Publishing Group. https://doi.org/10.1038/mp.2017.47

Tasic, B., Menon, V., Nguyen, T. N., Kim, T. K., Jarsky, T., Yao, Z., Levi, B., Gray, L. T., Sorensen, S. A., Dolbeare, T., Bertagnolli, D., Goldy, J., Shapovalova, N., Parry, S., Lee, C., Smith, K., Bernard, A., Madisen, L., Sunkin, S. M., Hawrylycz, M., Koch, C., & Zeng, H. (2016). Adult mouse cortical cell taxonomy revealed by single cell transcriptomics. *Nature Neuroscience*, *19*(2), 335–346. https://doi.org/10.1038/nn.4216

Van Strien, N. M., Cappaert, N. L. M., & Witter, M. P. (2009). The anatomy of memory: An interactive overview of the parahippocampal- hippocampal network. In *Nature Reviews Neuroscience* (Vol. 10, Issue 4, pp. 272–282). Nature Publishing Group. https://doi.org/10.1038/nrn2614

Whittaker, R. G., Turnbull, D. M., Whittington, M. A., & Cunningham, M. O. (2011). LETTER TO THE EDITOR Impaired mitochondrial function abolishes gamma oscillations in the hippocampus through an effect on fast-spiking interneurons. *A JOURNAL OF NEUROLOGY Advance Access*. https://doi.org/10.1093/brain/awr018

Whittington, M. A., Traub, R. D., Kopell, N., Ermentrout, B., & Buhl, E. H. (2000). Inhibition-based rhythms: Experimental and mathematical observations on network dynamics. *International Journal of Psychophysiology*, *38*(3), 315–336. https://doi.org/10.1016/S0167-8760(00)00173-2

Witter, M. P., Wouterlood, F. G., Naber, P. A., & Van Haeften, T. (2006). Anatomical Organization of the Parahippocampal-Hippocampal Network. *Annals of the New York Academy of Sciences*, *911*(1), 1–24. https://doi.org/10.1111/j.1749-6632.2000.tb06716.x

Wong-Riley, M. T. T. (1989). Cytochrome oxidase: an endogenous metabolic marker for neuronal activity. In *Trends in Neurosciences*. https://doi.org/10.1016/0166-2236(89)90165-3

Zeisel, A., M͡oz-Manchado, A. B., Codeluppi, S., Lönnerberg, P., Manno, G. La, Juréus, A., Marques, S., Munguba, H., He, L., Betsholtz, C., Rolny, C., Castelo-Branco, G., Hjerling-Leffler, J., & Linnarsson, S. (2015). Cell types in the mouse cortex and hippocampus revealed by single-cell RNA-seq. *Science*, *347*(6226), 1138–1142. https://doi.org/10.1126/science.aaa1934

Zhang, S., Schonfeld, F., Wiskott, L., & Manahan-Vaughan, D. (2014). Spatial representations of place cells in darkness are supported by path integration and border information. *Frontiers in Behavioral Neuroscience*, *8*(JUNE), 222. https://doi.org/10.3389/fnbeh.2014.00222